Research paper

Grasp analysis and optimal design of robotic fingertip for two tendon-driven fingers

Huixu Dong [a,*], Ehsan Asadi [a], Chen Qiu [b], Jiansheng Dai [b], I-Ming Chen [a]

[a] Robotics Research Centre, Nanyang Technological University, 50 Nanyang Avenue, Singapore
[b] Centre for Robotics Research, King's College London, London, United Kingdom

ARTICLE INFO

ABSTRACT

In this work, we focus on building the model of optimization design of the fingertip to evaluate the best fingertip shape and determining the size range of objects grasped by fingertips steadily. We describe the effect of fingertip dimension on the stability of fingertip grasp, while other existing works mostly paid close attention to stability analysis for existing fingertip designs or prototypes. First, we elaborate on a versatile force-form analysis approach to quantifying the grasp stability by constructing a series of mathematical models under rolling constraints. Second, the best performing fingertip shape is indicated for realizing stable fingertip grasps. Next, the relations between the dimension of the fingertip, the size of objects, and the posture of the fingertip relative to a stable contact point are expressed by mathematical formulations in geometric constraints. Finally, an under-actuated gripper with two 3-link fingers is designed and performs practical experiments to demonstrate for verifying the presented analysis and models.

© 2018 Elsevier Ltd. All rights reserved.

1. Introduction

Most of robots used in practical applications can perform stable grasps [1]. The robotic grippers are required to be all-purpose and capable such as to perform stable grasps and manipulations with a various size range of objects, while cost is always an issue to enable robotic grippers to be refined into products. To moderate these limitations, researchers have proposed under-actuated robotic grippers with tendon-driven mechanisms (TDMs) which are highly effective against enveloping grasp but are usually limited to the specific fingertip grasp task [2]. In practical applications, the fingertip grasp is a pivotal capability of developed grippers [3,4], since it is performed almost as frequently as an enveloping grasp [4–7]. The performance of an under-actuated gripper significantly depends on the design rather than the control method [7–9], and it is essential for optimization design of two-finger grippers with TDMs so that the gripper can realize stable fingertip grasps.

The grasp stability for control purposes is the tendency of the points of contact to return to their original locations in response to a disturbance [10]. However, from the application perspective, we consider the fingertip grasp as a stable grasp, if two fingertips could grip the object laying on a table and carry it till the object does not touch the tabletop, while the object remains between fingertips after the gripper is moved up a certain distance. Regardless of grasp manners, the stability of grasping objects is very important, as it indicates whether the grasp is successful or not. It is well-known that the dimension of fingertip has influences on a fingertip grasp stability such as the curvatures of contact surfaces [11]. Therefore, during the period of designing a well-functioning under-actuated robotic gripper, the optimization design of fingertip must

---

* Corresponding author.
E-mail address: dong0076@e.ntu.edu.sg (H. Dong).

be considered as a critical design criterion. This work tries to determine the dimension of fingertips of an under-actuated robotic gripper with two 3-link fingers for realizing a more stable fingertip grasp and then explore the size range of objects could be grasped steadily by fingertips under the precondition that the friction force counteracts the gravity of the object.

There are two main kinds of versatile methods describing the stability of fingertip grasp. One is that the stability of fingertip grasp is analyzed based on potential energy. For example, Funahashi et al. [12] presented a method of optimizing the quasi-static equilibrium equations by the equivalence of elastic system to analyze a fingertip grasping stability. Yamada et al. [13] discussed the static stability of a planar object grasped by multi-fingers based on the grasp stiffness matrix. A grasp stiffness matrix including the effect of contact surface geometry and contact condition on the grasp stability was derived in [14]. Also, the same authors used the partial derivative of the matrix to analyze the effect of the grasp parameters on the grasp stability through the eigenvalues and eigenvectors of the stiffness matrix [15]. The other is that the bound constraints of the contact space are applied to exploring a fingertip grasp stability depending on force/form closures. Rimon et al. developed a mobility theory including curvature effects of fingers and object for realizing a stable grasp based on the grasp form closure [16,17]. They used the polyhedral bounds regarding contact forces, surface normal, the surface curvature at the contacts to verify the effect of the curvature of contact surface on grasp stability according to the grasp force closure [18].

Here we summarize the main differences between our work and the prior works. In [12], they developed the model of coordinate transformation for an elastic system to analyse the grasp stability based on the potential energy. [13–16,18] also used the potential energy method to discuss the grasp stability. [16,18] considers the stability of an object supported by several frictionless contacts in a potential field. However, they did not study a specific case for a fingertip grasp with friction for practical grasp applications. Moreover, the contact force was not considered as an effective factor on grasp stability. While the model of potential energy based on the stiffness matrix are not novel, we have applied this model to analysis a new case of a stable two-fingertip grasp with friction by an under-actuated robotic gripper and to justify the choices made in the dimension parameters of the fingertip design, which is not studied in other works. The previous works [12–18] mostly analysed the stability of the existing design of fingertip or an available prototype rather than exploring the optimization design of fingertip according to the mathematical model. The focus of our work is to determine the best shape and dimension of a fingertip for design optimization to realize a stable grasp. We also discuss the effect of the radius of the fingertip on eigenvalues of stiffness matrix in practical applications, which is not studied in other work and this is the major contribution in Section 3. While previous works, such as [12,14,18], have analysed the stability of a general grasp problem by considering the curvature of both object and fingers at contact points, we focus on stability of fingertip grasp of objects laid on a flat surface where additional geometric and rolling constraints must be satisfied to realize a stable grasp. We formulate a mathematical model to explore the relation of the stability of a fingertip grasp and the dimension of the fingertip. The curvature of the contact interface affects the stable characteristics, and the dimension of gripper's fingertip affect the stable posture of the fingertip relative to the contact points and the underlying surface, as well as the size range of objects to be grasped steadily by fingertips.

Indeed, few works take into consideration of optimizing the design of a fingertip to realize stable fingertip grasp for an under-acuted robotic gripper. Montana et al. introduced the rolling constraints occurring between the fingertips of arbitrary shapes in detail [19]. Yoshida et al. utilized a mathematical and computational method to establish the model of pinching an object with arbitrary shape by two fingers with hemispherical ends [20]. Regarding the biomechanical perspective, Wu et al. [21] explored the contact interactions between fingertips and objects with different curvatures based on a finite element model. The rolling contact at the fingertip was considered to model the kinematics, statics and stiffness effect of a 3D grasp by describing the local shape of the fingertip and the object [22]. Hierarchical fingertip space was presented by Hang et al. [23] to enable optimization for both efficient grasp synthesis, and online finger gaiting. Regarding evaluating the grasp stability, the form closure (without force closure) cannot be adopted if a grasp is exerted by an under-actuated robotic gripper, as it is not practical for actuating individual phalanges independently [24–27].

Compared with a gripper with two parallel links with flat surfaces such as Robotiq [28], a two-finger gripper with TDMs cannot perform adaptive parallel grip. The limits on joints configuration of a tendon-driven gripper prevent the last joints to be parallel and to clamp a small object with flat fingertips. When a tendon-driven gripper with multiple joints carries out a fingertip grasp, the last joints drive fingertips to rotate continuously to touch an object to be grasped. Thus, if the surface of fingertip is flat or the curve radius is too large, it is not possible for using two fingers to clamp a small object laying on a desk or flat table. Employing a mathematical model to derive the dimension optimization of the fingertip depending on the force-form view (the friction and the dimension), to a lesser extent, would reduce the subjective considerations.

This work focuses on the analysis of fingertip grasp stability for optimizing the fingertip shape of under-actuated gripper from application perspective. Additionally, we determine the size range of objects could be grasped steadily by fingertips based on the dimension parameters and the grasp configuration of an under-actuated robotic gripper. The outline of the work is described below. Based on the force-form view, we discuss the grasping stability of fingertips. The potential energy can be used to determine the optimized shape of fingertip for realizing stable fingertip grasp. The grasping configuration of under-actuated gripper and the dimension of fingertip in the geometric constraints are applied to obtaining the sizes of objects that are grasped steadily. Specifically, the models of contact force and fingertip contact equivalent model are first built under the rolling constraints. Subsequently, we elaborate on the method of potential energy to quantify the grasp stability by a series of contact definitions for obtaining the mathematical model between the dimension of the fingertip and the grasp stability. Then, we indicate the optimization design of fingertip according to the rolling constraints for realizing a

stable fingertip grasp. Next, we present the corresponding formulations that express the relation between the dimension of a fingertip, the size of the object and the posture of the fingertip relative to a stable contact point in geometric constraints. Finally, an under-actuated gripper with two 3-link fingers is designed and fabricated according to the given model, and practical experiments are demonstrated to assess the presented model and analysis. We highlight the contributions of our work here.

(1) We elaborate on a versatile force-form analysis approach to quantifying fingertip grasp stability by constructing a series of mathematical models under rolling constraints.
(2) The mathematical derivations based on the model of the stable fingertip grasp under the rolling constraints provide the theoretical evidence concerning the fingertip design approach.
(3) The geometric relations between the dimension of the fingertip, the size of objects, and the posture of the fingertip relative to a stable contact point are expressed by mathematical formulations. The best performing fingertip shape is indicated as well that meets geometric constraints for realizing stable grasps.
(4) The formulation could help researchers in related fields for designing fingertip or evaluating fingertip grasping performances, such as a grasp stability, as well as to follow the research line and to further investigate new control strategies.
(5) A gripper with two 3-link fingers is designed based on the given analysis and deployed for practical experiments to demonstrate and to verify the performance.

The following contents of the paper include five sections. Section 2 concentrates on building the model of fingertip grasp using the force-form view under rolling constraints. Section 3 presents the derivations of fingertip dimension optimization for realizing stable fingertip grasps. The size ranges of objects grasped by fingertips steadily are determined based on the derivational conclusion regarding a fingertip dimension in the last section, which is described in Section 4 in detail. The fingertip grasp experiments are performed, and the corresponding discussions are provided in Section 5. Finally, conclusions are drawn in Section 6.

2. Model construction of fingertip grasp based on the force-form view

While previous works, such as the one by Funabashi, have analyzed the stability of a general grasp problem by considering the curvature of both object and fingers at contact points, we focus on stability of fingertip grasp of objects laid on a flat surface where rolling constraints must be satisfied to realize a stable grasp due to a contact friction generated by the contact force. We formulate a mathematical model to explore the relation of the stability of a fingertip grasp and the dimension of the fingertip. The curvature of the contact interface affects the stable characteristics [14], and the dimension of gripper's fingertip affect the stable posture of the fingertip relative to the contact points and the underlying surface, as well as the size range of objects could be grasped steadily by fingertips. With the purpose of simplifying this problem, the incidental factors are ignored, and then the following preconditions are made.

• The range of coefficient of friction at contact points between a fingertip (rubber) and an object rests on 0.2–1.6. In this work, the friction coefficient between the fingertip (rubber) and an object is set to 0.5.
• The spring stiffness is not only sufficiently strong to keep the links return the initial positions overcoming the resistance without the actuator forces but also as low as possible in order to relieve the actuated force consumption.
• The tiny motion between fingers and an object keeps a quasi-static equilibrium with small external disturbances, and the dynamic characteristics of the fingertip grasp are left out.
• Robotic fingers and objects are assumed to be rigid bodies, and they are in frictional contact with only one point, without slip. A fingertip grasp satisfies rolling constraints due to friction contacts.
• The fingers cannot be rotated since the stiffness of the finger is strong enough.
• The contact surface of fingers is continuous and convex.
• The robotic gripper performs a 2-D fingertip grasp.
• The boundaries of the fingertip and the grasped object are at least twice continuously differentiable and the first order derivatives of the boundaries do not vanish anywhere.

2.1. The model of force/torque transmission for fingertip grasp

As a contact force has an important effect on the stability of fingertip grasp, we have to build the model of force transmission between an actuated force and contact force. In this work, an under-actuated robotic gripper with two 3-link fingers is regarded as an example to explore the fingertip grasp for optimizing the fingertip dimension. The force/torque transmission from the actuator to robotic fingers determines the grasping forces/torques that exert an object [29]. To obtain the relation of the tendon tension force and the joint torque, we establish the kinematics of tendon-driven mechanism, as shown in Fig. 1. Then, depending on the principle of virtual work [29], the following equation is obtained,

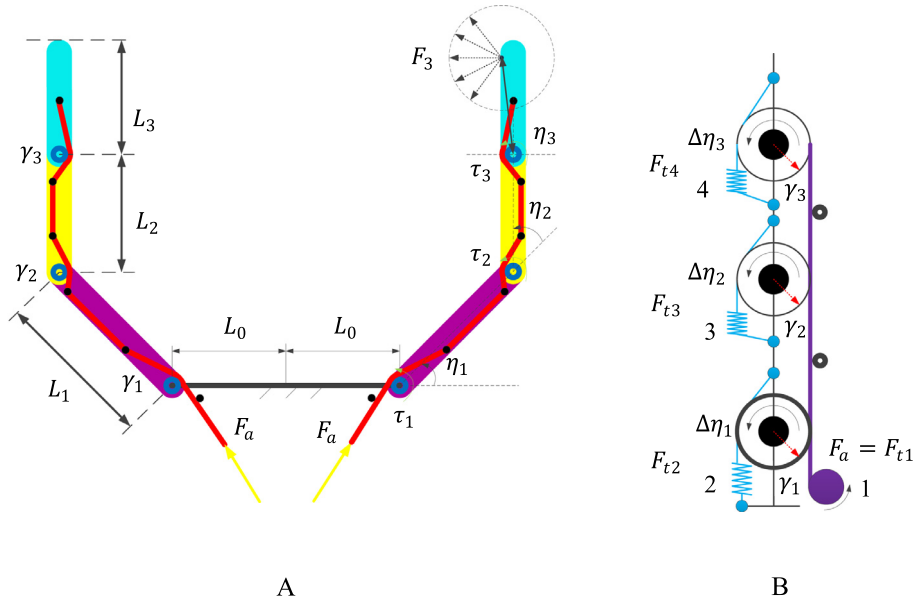$$\boldsymbol{\tau} = -\boldsymbol{J}_k^T \boldsymbol{F}_t \tag{1}$$

Fig. 1. A schematic of an under-actuated robotic gripper with tendon-driven mechanisms(A) and a schematic diagram of the tendon-driven mechanism of an under-actuated finger(B). The purple circle on the right represents an actuator, and the purple dots denote the idle mandrels (B); the tendon attached by the motor is regarded as the active tendon (1 in B)and others are considered as the passive tendons (2,3,4 in B). L_1, L_2, and L_3 represent the legnths of the first, the second and the third link, respectively. L_0 indicates the width of the half palm. η_i and $\Delta\eta_i$ denote the i-th joint anlge and joint angle variable, τ_i is the torque of the i-th joint ($i = 1, 2, 3$). F_3 denotes the fingertip contact force and it has many potential directions(the dotted arrows).

where J_k is the mapping Jacobian matrix from the force dimension to the torque dimension. Since the tension force is just considered, the negative sign is referred to the above equation. F_t represents the vector of tendon tension force, which is continuously positive since all the tendons cannot generate negative tension force. τ is the joint torque vector.

The idlers are applied to compressing tendons such as to ensure that the moment arm of the joint torque is the radius of joint. Referred to Fig. 1(B), an under-actuated finger has four tendons in the desired design, including one active tendon and three passive ones. The mapping Jacobian matrix J_k is obtained based on the following principle. The elements of the mapping Jacobian matrix are determined by the rotational direction of the joint axes and the tendon route. But in fact, the primary line transformation of the mapping Jacobian matrix does not affect on the function of the mechanism. That is, the mapping Jacobian matrix J_k of elementary transformation is equivalent. Thus, the definition of direction for the joints makes no difference to the tendon-driven mechanism. For instance, the positive direction of rotational joint is defined to be pointing out of the paper; the mapping Jacobian matrix J_k is described as follows,

$$J_k^T = \begin{bmatrix} \gamma_1 & -\gamma_1 & 0 & 0 \\ \gamma_2 & 0 & -\gamma_2 & 0 \\ \gamma_3 & 0 & 0 & -\gamma_3 \end{bmatrix}. \tag{2}$$

As shown in Fig. 1, the tendon tension force F_t is presented by

$$F_t = \begin{bmatrix} F_{t1} \\ F_{t2} \\ F_{t3} \\ F_{t4} \end{bmatrix} = \begin{bmatrix} F_a \\ -k_1\gamma_1\Delta\eta_1 \\ -k_2\gamma_2\Delta\eta_2 \\ -k_3\gamma_3\Delta\eta_3 \end{bmatrix} \tag{3}$$

where $F_{ti}(i = 1, 2, 3, 4)$ represents the tension force of each tendon and γ_i denotes the radius of the ith joint, $i = 1, 2, 3$. $k_i(i = 1, 2, 3, 4)$ are the stiffness of torque spring for the joint 1, 2, or 3, respectively. F_a indicates the tension force of the active tendon and $\Delta\eta_i(i = 1, 2, 3)$ are the variations of joint angles with respect to the initial values $\frac{\pi}{4}, \frac{\pi}{4}, 0$ for η_1, η_2 and η_3, correspondingly. From Eq. (3), we can obtain the following equation:

$$\tau = \begin{bmatrix} \tau_1 \\ \tau_2 \\ \tau_3 \end{bmatrix} = \begin{bmatrix} F_a\gamma_1 + k_1\gamma_1^2\Delta\eta_1 \\ F_a\gamma_2 + k_2\gamma_2^2\Delta\eta_2 \\ F_a\gamma_3 + k_3\gamma_3^2\Delta\eta_3 \end{bmatrix}. \tag{4}$$

The transmission model between contact forces and joint torques can be calculated depending on the principle of virtual work as follows,
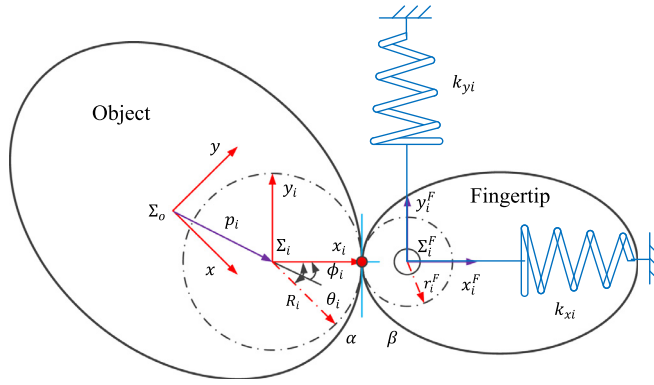
$$\tau = J_i^T F_i \tag{5}$$

Fig. 2. Fingertip friction grasp with one contact.

where J_i is the mapping Jacobian matrix from the contact force space to the joint torque space for an under-actuated finger with three links, and F_i denotes the force of the ith contact point regarding the fixed palm frame of reference. M_3 is the moment arm of the torque τ_3. The magnitude of the applied torque τ_3 is presented as:

$$|\tau_3| = |F_3 M_3|. \tag{6}$$

Due to the low speed movement and the light quality of the fingers compared with F_a, the dynamic properties of the gripper will not be analysed and the grasp maintains the static equilibrium [30]. Thus, combined Eqs. (4) and (6), the contact force F_3 is described by

$$F_3 = \frac{F_a \gamma_3 + k_3 \gamma_3^2 \Delta \eta_3}{M_3}. \tag{7}$$

As a standard mechanical part, the stiffness k_i is a constant. Since the actuated force F_3 is far larger than the spring tension force, the contact force can be simplified as follows,

$$F_3 = F_a \frac{\gamma_3}{M_3}. \tag{8}$$

2.2. The contact equivalent model for fingertip grasp

There exist three pre-conditions for constructing the equilibrium equations. First, the friction force can counteract the gravity of grasped object sufficiently. In other words, when the external disturbance occurs, such stiffness generated by the contact forces can maintain a static equilibrium state. Second, a set of arcs with different curvatures can consist of any curve and the ends of arcs are tangent to each other. Third, with the local curve explored, it is equivalent to an arc. α and β represent the contact arcs of the grasped object and fingertip, respectively, as shown in Fig. 2. The differential mechanism of robotic gripper distributes torques generated by an actuator to the two fingers such that robotic fingers have compliant characteristics within a certain range. In other words, the passive mechanism can be equivalent to an elastic mechanism in action effects [22,31,32]. Based on these three conditions, we set up the corresponding coordinate frames to describe the stability of fingertip grasp, as seen in Fig. 2.

The origin of the object frame of reference Σ_O is attached to the object center of mass and its y axis is perpendicular to the horizontal plane where the object is put. The contact curve of the grasped object is approximated by an arc with a radius R_i. The curvature center of the arc α is set as the origin of the coordinate frame Σ_i of the contact point and the x_i axis of Σ_i is along the normal of the contact point outwards. Similarly, an arc with the radius r_i^F ($r_i^F > 0$) at the contact surface of fingertip can take the place of the contact curve of fingertip. Moreover, the curvature center of the arc β is regarded as the origin of the fingertip frame of reference Σ_i^F and the direction of the x_i^F axis is the same as that of Σ_i. As to the relation between Σ_O and Σ_i, the displacement t_i, including the translation p_i and the rotation θ_i, is essential from Σ_O to Σ_i, as illustrated in Fig. 2. ϕ_i denotes the intersection angle of the translation p_i and the x_i axis.

The tangential force is generated due to the frictional contact between the fingertip and the object. Thus, any infinitesimal displacement for the grasped object results in a rolling contact and the fingertips can store potential energy by a compliant mechanism that is replaced by the virtual linear springs for an under-actuated gripper. In terms of a linear spring, it is characterized by a stiffness constant k_i and the orientation pointing to the axis of Σ_i^F. k_{xi} and k_{yi} represent the stiffness constants of virtual spring along the x_i^F and y_i^F axes, respectively. Besides, the potential energy also can be decomposed along the x_i^F and y_i^F axes.

We explore the relationship between the displacement at the origin of Σ_O and the compression δ_i [12]. Due to the external disturbance, the infinitesimal translation (x, y) and rotation ζ occur at the origin of Σ_O. The displacement at p_i,
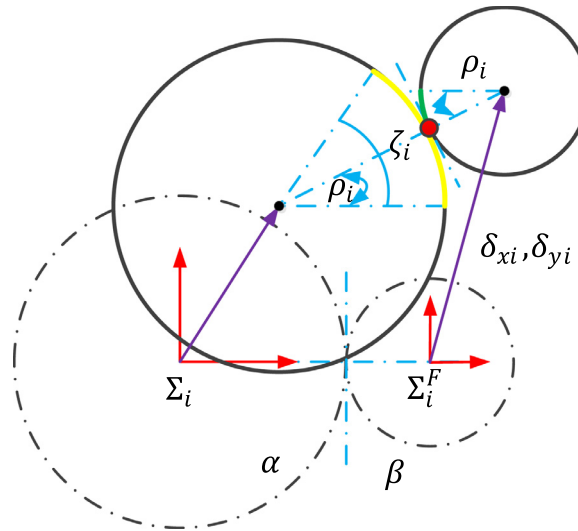
Fig. 3. The rolling motion of the fingertip and the grasped object under the tiny external disturbance. δ_{xi} and δ_{yi} denote the elastic compressions along the x and y axes with respect to the contact frame of reference Σ_i^F for the finger, respectively. ρ_i indicates the rotational angle of the fingertip and ζ_i represents the rotational angle for the grasped object.

which is the position of the origin of Σ_i, is represented by

$$(x, y)^T + (Rot(\zeta) - I_2) p_i \tag{9}$$

where I_2 is a 2×2 identity matrix, and $Rot(\zeta)$ is a rotation matrix represented by

$$Rot(\cdot) = \begin{bmatrix} cos(\cdot) & -sin(\cdot) \\ sin(\cdot) & cos(\cdot) \end{bmatrix}. \tag{10}$$

By transforming the displacement (x, y, ζ) in Σ_O into the displacement (x_i, y_i, ζ_i) in Σ_i, we obtain an equation as follows,

$$\begin{pmatrix} x_i \\ y_i \end{pmatrix} = Rot(-\theta_i)\left(\begin{pmatrix} x \\ y \end{pmatrix} + (Rot(\zeta) - I_2) p_i \right)$$
$$\zeta_i = \zeta \tag{11}$$

Because of the equation

$$p_i = (|p_i| \cos(\theta_i \mp \phi_i), |p_i| \sin(\theta_i \mp \phi_i)) \tag{12}$$

we can obtain the following equations:

$$x_i = x \cos\theta_i + y \sin\theta_i + p_i(\cos(\zeta - \phi_i) - \cos\phi_i);$$
$$y_i = -x \sin\theta_i + y \cos\theta_i + p_i(\sin(\zeta - \phi_i) + \sin\phi_i) \tag{13}$$

According to the rolling constraints, as illustrated in Fig. 3, the equations are provided as follows:

$$R_i + r_i^F + \delta_{xi} = \left(R_i + r_i^F \right) \cos\rho_i + x_i \tag{14}$$

$$\delta_{yi} = y_i + \left(R_i + r_i^F \right) \sin\rho_i \tag{15}$$

$$r_i^F \rho_i = R_i(\zeta_i - \rho_i). \tag{16}$$

(x_i, y_i) represents the infinitesimal translation ζ_i indicates the rotation. Substituting Eq. (13) into Eqs. (14) and (15), we can obtain the relation equations between the elastic compression $(\delta_{xi}, \delta_{yi})$ and the displacement (x, y, ζ) in the object frame of reference. Therefore, the compression δ_{xi} and δ_{yi} is given by

$$\delta_{xi} = x \cos\theta_i + y \sin\theta_i + p_i P_{B1} + P_{B2} \tag{17}$$

with $P_{B1} = \cos(\zeta - \phi_i) - \cos\phi_i$ and $P_{B2} = (R_i + r_i^F)(\cos\gamma_i - 1)$;

$$\delta_{yi} = -x \sin\theta_i + y \cos\theta_i + p_i P_{C1} + P_{C2} \tag{18}$$

with $P_{C1} = \sin(\zeta - \phi_i) + \sin\phi_i$ and $P_{C2} = (R_i + r_i^F) \sin\gamma_i$;

$$\rho_i = \frac{R_i \zeta}{R_i + r_i^F}. \tag{19}$$

3. Determination of fingertip dimension for stable fingertip grasps

3.1. Evaluation of fingertip grasp stability under rolling constraints

According to the model of force transmission (2.1) and the contact equivalent model (2.2), we can determine the effect of fingertip dimension on a fingertip grasp stability. The rolling motion of the fingertip and the grasped object, including the infinitesimal translation and rotation, occurs due to the tiny external disturbance. The static equilibrium means the sum of all contact forces is equal to zero. Meanwhile, a grasp stability is equivalent to the suitable stiffness exerted on the grasped object, which comes from the stiffness of the tendons or active stiffness control of the fingers [32]. We focus on the stiffness from an under-actuated robotic gripper based on the energy conservation. When the two under-actuated fingers are applied to performing the fingertip grasp, the total potential energy of the elastic system is given by

$$U = \sum_{i=1}^{2} \left\{ \frac{1}{2} k_{xi} (\delta_{xi} + \delta_{oxi})^2 + \frac{1}{2} k_{yi} (\delta_{yi} + \delta_{oyi})^2 \right\}, \tag{20}$$

where U stored in the elastic system is the sum potential energy of two fingers. Moreover, δ_{oxi} and δ_{oyi} denote the initial compressions at the static equilibrium state, δ_{xi} and δ_{yi} denote the elastic compressions along the x and y axes with respect to the contact frame of reference Σ_i^F for the finger, respectively. k_{xi} and k_{yi} represent the stiffness constants along the horizontal and vertical directions. $f_{xi} = k_{xi}\delta_{oxi}$ and $f_{yi} = k_{yi}\delta_{oyi}$ are the initial grasp forces. In term of f_{xi}, we set the direction that points to the interior of the fingertip is positive along the x_i^F axis of Σ_i^F. When the gripper grasps an object, the tangent force f_{yi} generated by rolling constraint performs a pulling force against the object gravity. The direction opposite to the gravity is regarded as the positive direction for f_{yi} along the y_i^F axis of Σ_i^F.

In fact, the potential function U is twice continuously differentiable. To simplify the calculation, we describe Eq. (20) as the Taylor expansion of the potential function U at the equilibrium configuration in the matrix form as follows:

$$U = U(0) + X^T \nabla U|_{(0)} + \frac{1}{2} X^T H|_{(0)} X + \dots, \tag{21}$$

where $X = (x, y, \zeta)^T$ is the transpose of the displacement of the grasped object. Hamiltonian operator ∇ is expressed as $(\frac{\partial}{\partial x} I + \frac{\partial}{\partial y} J + \frac{\partial}{\partial \zeta} K)$, which I, J and K represent the unit vectors along the orientations of x, y and ζ, or $(\frac{\partial}{\partial x} \ \frac{\partial}{\partial y} \ \frac{\partial}{\partial \zeta})^T$, respectively. H represents the Hessian matrix.

The grasp is stable if and only if the potential energy U achieves the minimum value locally at the equilibrium state [12,32,33]. Specifically, the grasp is in the equilibrium configuration initially, thus, $\nabla U|_{(0)} = 0$. The sufficient condition that the potential function U is locally minimum is that $H|_{(0)}$ is a positive definite. In other words, all the eigenvalues of the matrix $H|_{(0)}$ must be positive, however direct determination of the eigenvalues is difficult due to the complexity of formulation. The matrix $H|_{(0)}$ can be characterized by the specific elements as follows,

$$H|_{(0)} = \begin{bmatrix} K_{xx} & K_{xy} & K_{x\zeta} \\ K_{yx} & K_{yy} & K_{y\zeta} \\ K_{\zeta x} & K_{\zeta y} & K_{\zeta \zeta} \end{bmatrix}. \tag{22}$$

Thus, we can obtain the elements,

$$K_{xx} = \sum_{i=1}^{2} \left(k_{xi} c_i^2 + k_{yi} s_i^2 \right),$$

$$K_{xy} = K_{yx} = \sum_{i=1}^{2} \left(k_{xi} - k_{yi} \right) c_i s_i,$$

$$K_{x\zeta} = K_{\zeta x} = \sum_{i=1}^{2} \left(k_{xi} l_{yi} c_i - k_{yi} l_{xi} s_i \right),$$

$$K_{yy} = \sum_{i=1}^{2} \left(k_{xi} s_i^2 + k_{yi} c_i^2 \right),$$

$$K_{y\zeta} = K_{\zeta y} = \sum_{i=1}^{2} \left(k_{xi} l_{yi} s_i + k_{yi} l_{xi} c_i \right),$$

$$K_{\zeta \zeta} = \sum_{i=1}^{2} \left(k_{xi} l_{yi}^2 + k_{yi} l_{xi}^2 - f_{xi} \left(l_{xi} - \frac{R_i r_i^F}{R_i + r_i^F} \right) + f_{yi} l_{yi} \right),$$
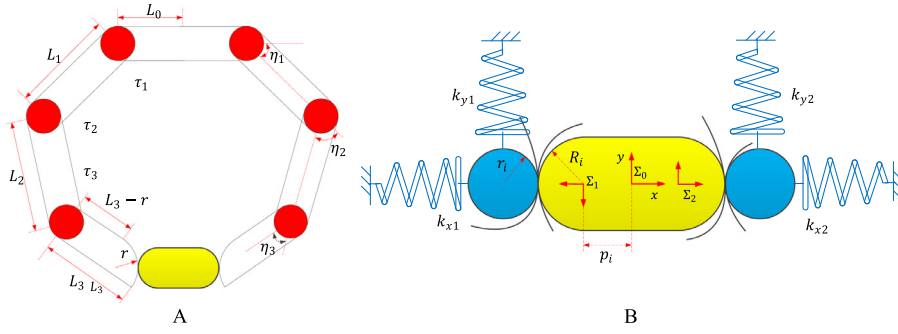
Fig. 4. (A) The example of fingertip grasp; (B) the detail of (A). $L_1, L_2,$ and L_3 represent the legnths of the first, the second and the third link, respectively. L_0 indicates the width of the half palm. η_i denotes the i-th joint anlge and τ_i is the torque of the i-th joint ($i = 1, 2, 3$). Σ_i denotes the coordinate frame of the i-th contact point ($i = 1, 2$).

and $l_{xi} = p_i \cos \phi_i + R_i$, $l_{yi} = p_i \sin \phi_i$, $c_i = \cos \theta_i$, $s_i = \sin \theta_i$, l_{xi} and l_{yi} represent the components of the distance that is between the object frame of reference and the contact point along the x_i and y_i axes of Σ_i.

In this work, we merely focus on the effect of the dimension and shape of the fingertip on the grasp performance. Thus, the curvature of contact is the uppermost important factor such that other non-primary factors are neglected. According to the symmetrical grasp characteristics of fingertips, the x_i axis of contact points is along the x axis of the object frame of reference Σ_O, namely, while it is without the translation along the y axis and the rotation of ϕ, as depicted in Fig. 4. Then, we have $\phi_1 = \phi_2 = 0$, $\theta_1 = 0$ and $\theta_2 = \pi$ (Fig. 4) along the horizontal direction, which leads to $l_{yi} = 0$ and $s_i = 0$. So the following non-diagonal elements of the matrix $H|_{(0)}$ become zero

$$K_{xy} = K_{yx} = \sum_{i=1}^{2} (k_{xi} - k_{yi}) c_i s_i = 0,$$

$$K_{x\zeta} = K_{\zeta x} = \sum_{i=1}^{2} (k_{xi} l_{yi} c_i - k_{yi} l_{xi} s_i) = 0,$$

Also, because of the two same fingertips, we have $k_{y1} = k_{y2} = k_y$. Moreover, considering symmetric objects then $R_1 = R_2 = R$, and $p_1 = p_2 = p$, as shown in Fig. 4. Finally, the other two non-diagonal elements of the matrix $H|_{(0)}$ become zero as following,

$$K_{y\zeta} = K_{\zeta y} = \sum_{i=1}^{2} (k_{xi} l_{yi} s_i + k_{yi} l_{xi} c_i) = k_y (p \cos 0 + R) \cos 0 + k_y (p \cos 0 + R) \cos \pi = 0,$$

Accordingly, the matrix $H|_{(0)}$ becomes

$$H|_{(0)} = \begin{bmatrix} K_{xx} & 0 & 0 \\ 0 & K_{yy} & 0 \\ 0 & 0 & K_{\zeta\zeta} \end{bmatrix}. \tag{23}$$

Hence, the eigenvalues of the matrix $H|_{(0)}$ are K_{xx}, K_{yy} and $K_{\zeta\zeta}$, respectively. The matrix $H|_{(0)}$ is ensured to be positive definite if and only if all the eigenvalues K_{xx}, K_{yy} and $K_{\zeta\zeta}$ are greater than zeros as follows ($i = 1$ or 2):

(a) $K_{xx} = \sum_{i=1}^{2} (k_{xi} c_i^2 + k_{yi} s_i^2) = \sum_{i=1}^{2} (k_{xi} c_i^2) > 0$;

(b) $K_{yy} = \sum_{i=1}^{2} (k_{xi} s_i^2 + k_{yi} c_i^2) = \sum_{i=1}^{2} (k_{yi} c_i^2) > 0$;

(c) $K_{\zeta\zeta} = \sum_{i=1}^{2} (k_{yi} l_{xi}^2 - f_{xi} (l_{xi} - \frac{R_i r_i^F}{R_i + r_i^F})) > 0$

According to the above assumptions, the conditions a) and b) are satisfied. Thus, the condition c) has to be discussed further. To ensure $K_{\zeta\zeta} > 0$, the following equation can be given as

$$\frac{R_i r_i^F}{R_i + r_i^F} > l_{xi} - \frac{k_{yi} l_{xi}^2}{f_{xi}}.$$

The precondition of a grasp is that there is a point contact between the finger and grasped object. As for the arc α at the fingertip and the arc β at the grasped object, the corresponding curvatures at contact point are κ_i and κ_i^F, respectively. To
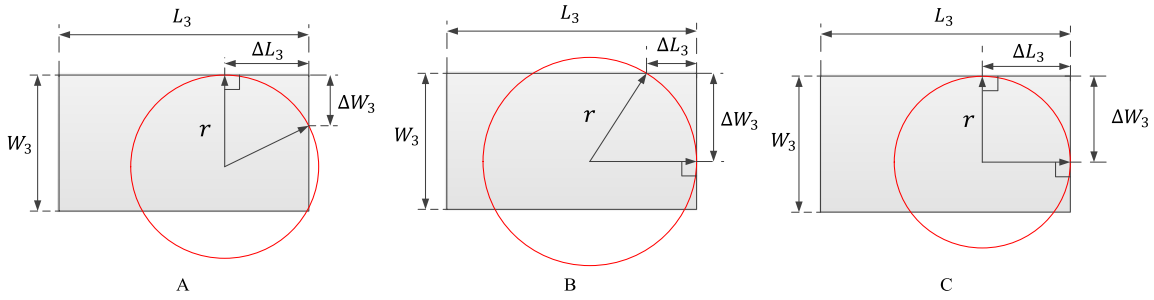
Fig. 5. The schematic combination of a circle (representing a finger's tip) with a rectangle (representing a finger's link) while being tangent to the edges of the rectangle. L_3 and W_3 represent the length and width of the finger, respectively; ΔL_3 and ΔW_3 denote the sizes of the part removed along the length and width edges, subjecting to $0 \leq \Delta L_3 \leq L_3$ and $0 \leq \Delta W_3 \leq W_3$ and $L_3 > W_3$. r is the radius of the circle.

ensure a point contact, we allow the condition to conform to $\kappa_i + \kappa_i^F > 0$ [19,34] . Due to $\kappa_i = \frac{1}{R_i}$ and $\kappa_i^F = \frac{1}{r_i^F}$, $\frac{1}{R_i} + \frac{1}{r_i^F} > 0$ is obtained. Besides, referring the assumptions above, r_i^F must be bigger than zero.

Setting $l_{xi} - \frac{k_{yi}l_{xi}^2}{f_{xi}} = M$, we have $1 > (\frac{1}{R_i} + \frac{1}{r_i^F})M$. There exist the three following cases for getting the range of r_i^F:

a. $M > 0$	i. $\frac{1}{M} - \frac{1}{R_i} > 0$, $r_i^F > \frac{R_i M}{R_i - M}$	
	ii. $\frac{1}{M} - \frac{1}{R_i} \leq 0$, $\frac{1}{r_i^F} \leq \frac{1}{M} - \frac{1}{R_i}$ (Disconfirm)	
b. $M < 0$	$\frac{1}{M} < 0 < \frac{1}{r_i^F} + \frac{1}{R_i}$;	
c. $M = 0$	$0 < \frac{1}{r_i^F} + \frac{1}{R_i}$.	

Combining a, b, and c, the interaction is $r_i^F > \frac{R_i M}{R_i - M}$, subjecting to $\frac{1}{M} - \frac{1}{R_i} > 0$ and $\frac{1}{r_i^F} + \frac{1}{R_i} > 0$ in order to realize a stable fingertip grasp. Thus, the radius of the fingertip must satisfy the value range. After obtaining the range of r_i^F, we discuss the effect of the value of the radius r_i^F on the eigenvalues in terms of $K_{\zeta\zeta}$ as follows,

$$K_{\zeta\zeta} = \sum_{i=1}^{2} \left(k_{yi}l_{xi}^2 - f_{xi}\left(l_{xi} - \frac{R_i r_i^F}{R_i + r_i^F} \right) \right) = \sum_{i=1}^{2} \left(k_{yi}l_{xi}^2 - f_{xi}l_{xi} + f_{xi}\frac{R_i}{\frac{R_i}{r_i^F} + 1} \right). \tag{24}$$

It is obvious that the larger the radius r_i^F of the fingertip is, the larger the eigenvalue $K_{\zeta\zeta}$ is. Thus, a fingertip with the larger radius makes a grasp more stable than one with a smaller radius. However, in a practical life, as hardware and kinematic constraints, the radius of the fingertip must be within a certain range and tend to the maximum value.

3.2. Best performing shape of a fingertip for realizing a stable fingertip grasp

From a morphological view, the outline of a human finger consists of circle and rectangle patterns. In this section, we approximate a finger's link as a rectangle with certain thickness W_3 and length L_3, and the finger's tip as a curve with a certain radius r, and the goal is to verify the best geometric relation between the finger's tip and finger's link for design purposes. Accordingly, various configurations of combining circles and a rectangle are explored, to determine the best shape of the fingertip based on the given analysis above through taking account of the fingertip grasp stability and the radius of fingertip.

Since a rolling constraint with frictional contact occurs during the period of a fingertip grasp, the transition point formed by different shapes must be the tangent point. Indeed, there are two tangent fashions between a circle and a rectangle, including a circle being tangent to the fixed length edge L_3 or the fixed width edge W_3. Fig. 5(A-B) illustrate two different configurations where fingertip's curve is tangent to only one of the edges of the link. However, the fingertip's curve should be tangent to both the length and width edges of the finger's link, as depicted in Fig. 5(C), which makes the rolling constraint occur when a robotic gripper performs a fingertip grasp. According to the geometric condition, the radius r is given as

$$r = \begin{cases} \Delta W_3, & 0 \leq \Delta W_3 \leq W_3 \\ \Delta L_3, & 0 \leq \Delta L_3 \leq L_3 \end{cases}. \tag{25}$$

Based on the conclusion drawn above, a larger radius r could result in a more stable fingertip grasp. The numerical magnitude of the radius r tends to be maximum. Referring to Eq. (25), the maximum value of r is equal to W_3 when W_3 is less than L_3.

To this end, the best fingertip shape for realizing a stable fingertip grasping must meet all geometric constraints given above. It should have an arc with the maximum allowable radius, which is equal to the width of the finger, and the arc also must be tangent to both of the length and width edges of finger. Fig. 6 indicate the best geometric configuration of fingertip
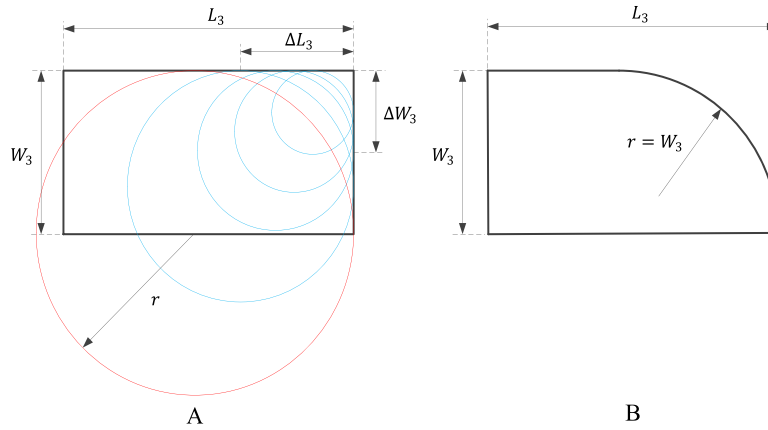
Fig. 6. Best geometric configuration of fingertip, in which the radius of the tip is taken as the maximum allowable value and the curve is tangent to the both edges of the link. All circles with varaible radius *r* are tangent to the length and width edges of the finger (A). The curve is tangent to the both length and width edges of the finger, and the radius of the fingertip is equal to the maximum allowable value, which is equal to the width of the finger(B).
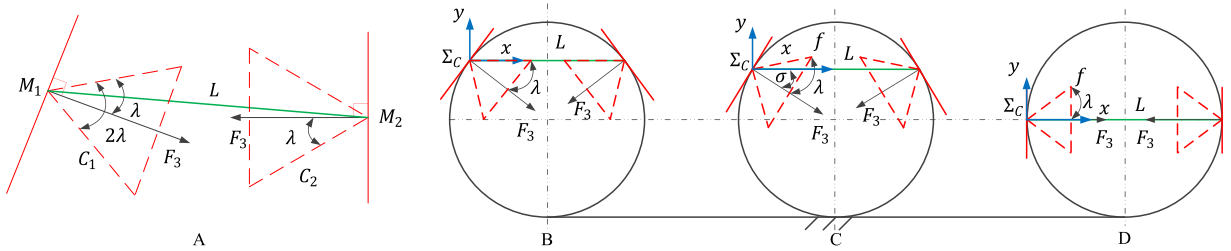

Fig. 7. Two opposite point grasp achieving a planar force closure for a fingertip grasp (A). The line jointing two contact points and the boundary lines of two friction cones are coincident (B). Such line is within the boundary lines of two friction cones (C). The line *L* and the horizontal line are coincident(D). N_1 and N_2 are the contact points for the contact normal force F_3. C_1 and C_2 denote the two friction cones with the friction angle λ. *L* is the line between the contact points M_1 and M_2.σ indicates the intersection angle between the direction of the contact force F_3 and the horizontal direction.Three cases of a two-point opposite grasp. Σ_C is the coordinate frame of the contact point with the *x* axis along the horizontal direction and the *y* axis along the vertical direction.

where the radius of the curve is increased to the maximum allowable value, while the curve is still tangent to the both edges of the link.

4. Determination of the sizes of objects under geometric constraints for stable fingertip grasps

A gripper cannot perform an enveloping grasp if the object to be grasped, is placed on a flat surface. In this case, the gripper has to use its fingertips to pick up an object. In this work, we just consider 2D planar objects. A circular object [7,25] and a rectangle object are considered as representative objects to explore a fingertip grasp due to the two reasons. The surfaces of circular and rectangle objects are convex so that each fingertip just has at most one contact point. Moreover, we refer to a circular object with just one variable (the radius *R*) and a rectangle object with two variables (the width O_w and the thickness O_t) as examples to simplify the geometrical model formulations and calculations. The models can be extended to objects with other shapes depending on the corresponding geometric constraints [35]. Also, the posture of fingertip relative to the contact point and the table surface, which is represented by the critical intersection angle φ between the third link and the flat plane, could be carried out by the dimension of fingertip and the sizes of objects for realizing a stable fingertip grasp.

To realize a static equilibrium state, the friction forces at contact points must counteract the gravity of grasped object, as shown in Fig. 7(C). The corresponding force equilibrium equation can be provided as

$$G = 2F_3\mu\cos\sigma, \tag{26}$$

where *G* represents the gravity of grasped object, μ denotes the friction coefficient of contact point and σ indicates the intersection angle between the direction of contact force and the horizontal direction. $\mu = \tan\lambda$, λ is the friction angle with $\lambda > \sigma$. Substituting Eq. (8) into Eq. (26), we can get the following equation,

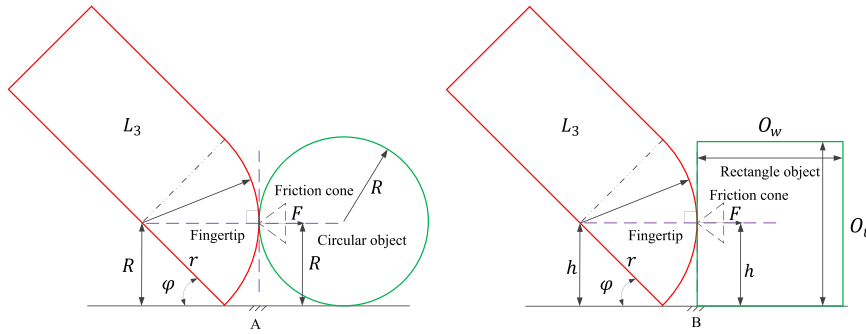$$G = \frac{2F_a r_3 \mu \cos\sigma}{M_3} . \tag{27}$$

Fig. 8. The relation between fingertip dimensions and the sizes of circular object (A) and rectangle object (B) for a stable grasp. The dased triangle represents the friction cone. F is the contact force.

4.1. Relation among the dimensions of fingertip, the grasp configuration and the size of circular object

A fingertip grasp with two fingers is regarded as two-point opposite grasp in a plane. For the two-point opposite grasp, the force closure plays a crucial role in realizing a stable grasp whether the gripper is under-actuated or not. The condition that achieves the grasp force closure is defined by [36]. Particularly, two point contacts with friction at M_1 and M_2 come into being a 2D force-closure grasp if and only if the segment $L(P_1P_2)$ points into the two friction cones strictly [36], as illustrated in Fig. 7. Among the three grasp configurations of (B), (C) and (D) in Fig. 7, (D) is the best grasp configuration for achieving a fingertip grasp stability. We use the grasp configuration of (D) as an example for circular objects to do the subsequent analysis, which allows a fingertip grasp about a circular object to achieve the best grasp stability. As the two fingertips are symmetrical, only one fingertip is applied to analyzing the fingertip grasp. Under the best force-closure form in Fig. 7(D), the relation among the size of a circular object, the dimension of fingertip and intersection angle is given by

$$R = r\sin\varphi \qquad (28)$$

with $\varphi = \pi - \eta_1 - \eta_2 - \eta_3$, as shown in Fig. 9. φ falls in a certain range: $\varphi_{min} < \varphi < \varphi_{max}$. The maximum allowable value φ_{max} of the intersection angle varies relative to the size of object. The minimum allowable value φ_{min} could approach zero if there is no limit on joint configurations of an under-actuated gripper, and φ_{max} could approach to 90° when the radius of circular object to be grasped is equal to the radius of the fingertip. Under the condition of satisfying Eq. (28), the size of circular object grasped is determined depending on the grasp configuration in Fig. 8(A) as follows,

$$2R = 2r\sin\varphi \qquad (29)$$

$$2R = 2L_0 - 2(L_3 - r)\cos\varphi + 2L_1\cos\eta_1 + 2L_2\cos(\eta_1 + \eta_2) - 2r. \qquad (30)$$

Indeed, Eqs. (29) and (30) are equivalent each other.

4.2. Relation among the dimension of fingertip, the grasp configuration and the size of rectangle object

As to a fingertip grasp of rectangle object, the grasp geometric relation is given by

$$h = r\sin\varphi, \qquad (31)$$

with $\varphi = \pi - \eta_1 - \eta_2 - \eta_3$, where h is the distance between a contact point and the horizontal line, as shown in Fig. 8(B). Due to the geometric constraint, h is not greater than the thickness O_t of the rectangle object ($O_t \geq r\sin\varphi$). We can obtain the range of the critical intersection angle φ as follows,

$$0 < \varphi \leq \sin^{-1}(O_t/r).$$

The maximum allowable value ($\varphi_{max} = \sin^{-1}(O_t/r)$) of the intersection angle varies with the size of grasped object changing. The minimum allowable value φ_{min} could be equal to zero if the hardware has no limitations. Fig. 9(B) indicates the geometric relation between the grasp configuration and the size of the grasped rectangle object. In order to realize a stable fingertip grasp, the dimension of rectangle object to be grasped must satisfy the inequation $O_t \geq r\sin\varphi$. Finally, the width O_w of the grasped object is expressed by the radius of the fingertip and the grasp configuration,

$$O_w = 2L_0 - 2(L_3 - r)\cos\varphi + 2L_1\cos\eta_1 + 2L_2\cos(\eta_1 + \eta_2) - 2r. \qquad (32)$$
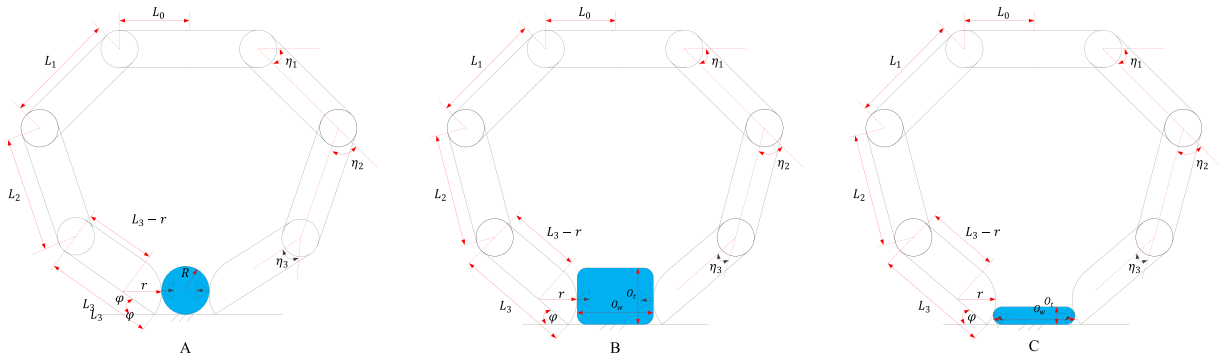
Fig. 9. The geometric relations of the grasp configurations and the sizes of a circular object(A) and a rectangle object (B). An unstable grasp case(C). The symbol implacations are the same as that of Fig. 4. The dased triangle represents the friction cone.
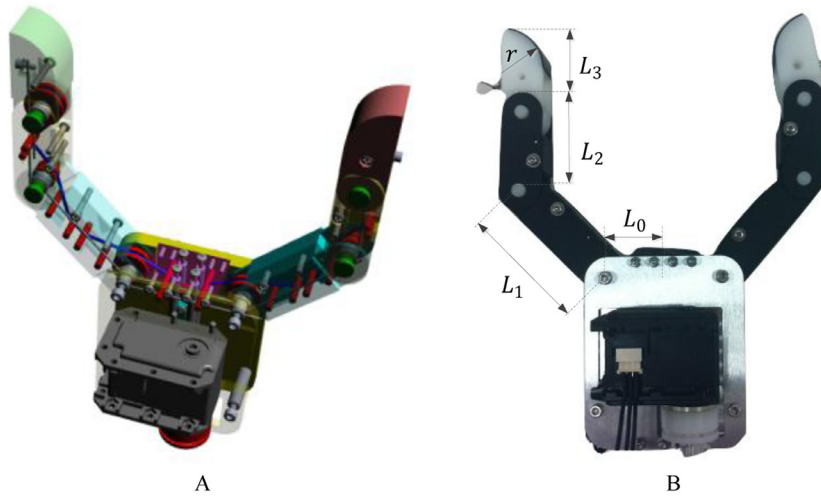

Fig. 10. The designed CAD model (A) and the gripper prototype (B). The dimensions of the under-actuated robotic gripper are given such as $L_1 = 55mm$, $L_2 = 35mm$, $L_3 = 25mm$, $L_0 = 22.5mm$ $r = 18mm$. The intial angles of the first, second, and third joints are $\frac{\pi}{4}, \frac{\pi}{4}$ and 0, respectively. r_3 represents the mandrel radius of the third joint, $r_3 = 8mm$. The minimal actuated force F_a of the active tendon is 86 N. μ denotes the friction coefficent of fingertip surface($\mu = 0.5$). 27 mm is regarded as the maximal moment arm M_3 of the third joint torque τ_3(max$(M_3)= \sqrt{r_3^2 + L_3^2}$).

5. Experiments and discussions

By taking account of the given stability analysis, a gripper is designed and fabricated to perform grasp experiments, as shown in Fig. 10, which is deployed in this experiment as an example to explore the influence of the fingertip dimension on a stable fingertip grasp for objects with different sizes. Fig. 10 also lists the parameters of the under-actuated gripper with two 3-link fingers. Without loss of generality, we have selected a set of 30 daily objects, which are used in offices and households, such as a pen, glass case, cell phone, USB drive, toothbrush, mouse, etc., for performing fingertip grasp experiments.

From Eq. (27), we can get the maximal gravity of object that can be lifted, $G = 25.5 \cos \delta$ (max$(M_3) = 27mm$, $\mu = 0.5$, $F_a = 86N$, $r_3 = 8mm$). Note that the friction coefficient μ between the fingertip (rubber) and an object (aluminium) is set to 0.5. For designing the fingertip, the r value is selected by using Eq. (28) ($r = R_{min}/ \sin \varphi_{min}$), and assuming O_t (min) $= R$(min) $=$ 10 mm and $\varphi_{min} = 35 \degree$degree, so as to enable fingertip grasp of objects with the thickness about 1 centimeter and higher. To realize a stable fingertip grasp, the intersection angle δ between the direction of contact force and the direction of horizontal line is close to zero, as mentioned above. The range of gravities of chosen objects, utilized in the experiments, falls in between of 0.2 N to 2 N approximately (Tables 1 and 2). Thus, the friction force of gripper is strong enough against the gravity of selected objects.

The objects are placed on a table, and then their dimensions are approximated by bounding boxes (the width and thickness O_w, O_t, respectively) that enclose objects as indicated in Tables 1 and 2 [4]. We set the thickness O_t as the distance between the plane and the top of the bounding box, and the width O_w as the length of the short side of the bounding box when an object rests on a flat table. As for a bounding box enclosing a circular object, the width O_w is the same as the thickness O_t that is equal to the diameter of circular object.

Table 1

The names, sizes, and intersection angles and gravities of objects used in the experiments with thicknesses less than the size of the fingertip, $O_t < 19$ mm. $\varphi_{measure}$ is measured manually for each test and $\varphi = \sin^{-1}(O_t/r)$ represents the critical intersection angle which is only applicable for small objects with $O_t/r < 1$. The information for unsuccessful grsap experiments are depicted in Boldtype. The objects are sorted according to the tickness O_t of the objects.

Items	Ballpoint pen	USB drive	Cell Phone	Sticky note	Plate	Color pen	Pin box	Glue	Clip box	Foam
Gravity(N)	0.272	0.204	1.324	0.546	1.967	0.356	0.525	0.632	0.657	0.821
O_t (mm)	**5.5**	**8**	**9**	10	**10**	12	12	15	15	17
O_w (mm)	**6**	**26**	**70**	19	**80**	12	20	15	24	27
$\varphi_{measure}$ (°)	**25**	**34**	**55**	27	**42**	35	30	35	30	35
φ (°)	**17.79**	**26.38**	**30**	33.75	**33.75**	41.81	41.81	56.44	56.44	70.81

Table 2

The names, sizes, and actual intersection angles and gravities of objects used in the experiments with thicknesses more than the size of the fingertip, $O_t > 19$ mm. $\varphi_{measure}$ is measured manually for each test and for these objects there is no limits on the intersection angle. The objects are sorted according to the width of the objects O_w (mm).

Items	TV controller	Scotch tape	Remote controller	Toothpaste	Light controller	Toy block	Tea box	Mouse	Card box	Soap
Gravity(N)	1.20	1.126	0.624	0.913	1.078	0.463	0.740	0.686	0.535	0.80
O_t (mm)	25	20	22	28	28	35	55	30	30	28
O_w (mm)	10	30	32	34	35	40	40	45	50	52
$\varphi_{measure}$ (°)	25	36	35	37	36	38	35	42	42	41
φ (°)	–	–	–	–	–	–	–	–	–	–

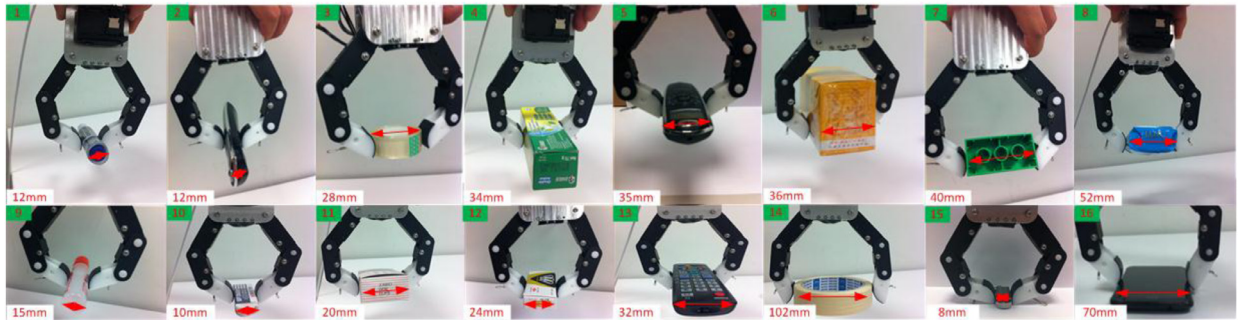| Items	Plug	Glass box	Stapler	Can	Hard disk	Milk box	Calculator	Biscuit box	Charger	Tape
Gravity(N)	0.668	0.951	1.028	1.918	1.807	1.654	0.946	1.748	2.146	0.865
O_t (mm)	30	32	27	30	25	45	25	30	25	20
O_w (mm)	55	55	55	64	70	75	75	80	95	102
$\varphi_{measure}$ (°)	44	45	43	52	52	64	64	69	73	75
φ (°)	–	–	–	–	–	–	–	–	–	–

Fig. 11. Samples of practical fingertip grasps of various objects with different shapes, widths and thicknesses. The numbers in white frames represent the widths of the grasped objects. The 15th (usb)and 16th (cellphone)cases show the unsuccessful grasps and other cases illustrate the successful grasps.

To perform the grasp experiments, we chose objects with the smallest dimension above 5 mm (e.g. Coins, etc.) and largest dimension shorter than 102 mm (e.g. Tapes, etc.). Practical fingertip grasp cases are illustrated in Fig. 11, which demonstrate stable fingertip grasps for these items. In terms of the experimental results, the gripper picks up 26 objects successfully while a ballpoint pen, cell phone, USB drive and a plate cannot be grasped with success. Here we can do the qualitative analysis regarding the results provided in Tables 1 and 2. According to the results, given in Table 1, the objects with around 10 mm thickness and higher are successfully grasped if the object width is less than 50 mm. For a cell phone and a plate, the width is too large in comparison with the thickness of objects. Specifically, for objects with low thickness and large width, the critical intersection angle is small but the actual intersection angle must be large to wrap fingers around the object, which results in an unsuccessful fingertip grasp. Concerning the under-actuated gripper with two 3-link fingers, the last joints cannot rotate enough angles so that the connection line of contact points falls into the interior area of two friction cones when the gripper grasps a flat object using fingertips, as shown in Fig. 9(C). For those objects with thicknesses larger than the radius of the fingertip, there are no geometric constraints on the intersection angle to realize successful fingertip grasp if the mechanism constraints are satisfied. As given in Table 2. the actual intersection angle for fingertip grasp is increased proportionally to the width of the objects.

Since the intersection angle is just one variable in experiments, we pay close attention to getting this variable when the gripper performs a fingertip grasp. For an object that cannot be picked up by the fingertips successfully, the measured intersection angle $\varphi_{measure}$ is more than the critical intersection angle ($\sin^{-1}(R/r)$ or $\sin^{-1}(O_t/r)$) derived by Eq. (28) or
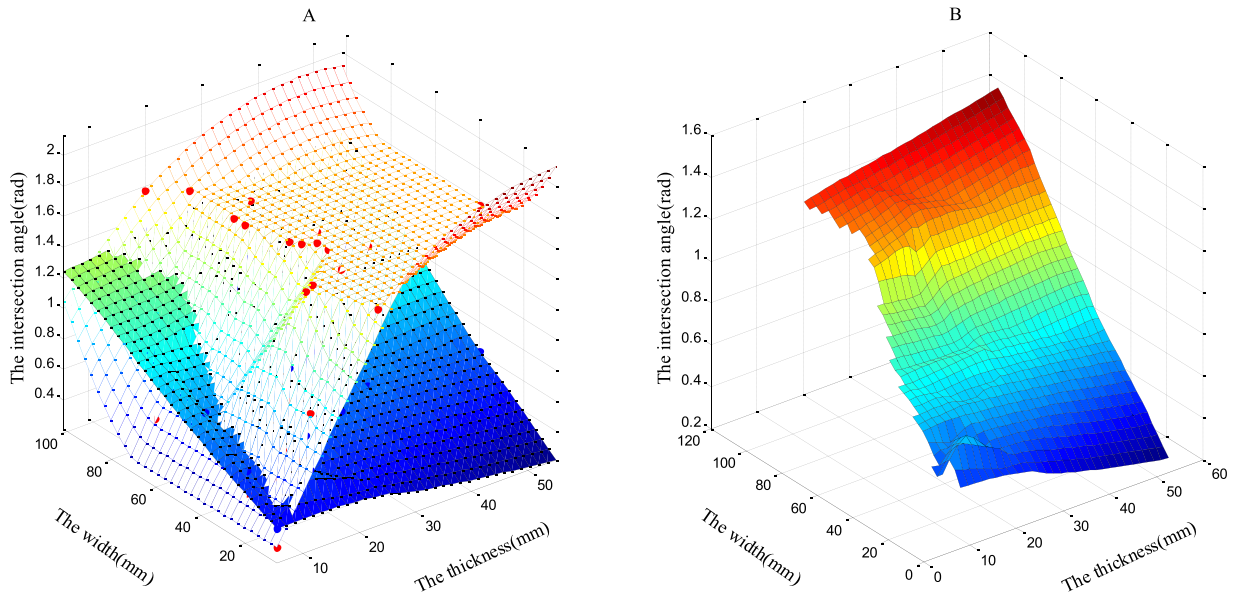
Fig. 12. The stable grasp space and unstable grasp space regarding intersection angles(A). The light-colored surface is fitted to the critical intersection angles, and the dark-colored surface is fitted via the measured intersection angles. The red and blue dots represent the critical and measured intersection angles of objects with different dimensions. The relation between the dimension of the objects and the corresponding intersection angles for successful fingertip grasps(B).

Eq. (31) when the fingertips touch an object. For realizing a stable grasp, the gripper must configure the suitable intersection angle φ for grasping an object with specific width O_w and the thickness O_t. We use discrete points to plot surfaces to have a better presentation of these geometric relations in Fig. 12. Specifically, the blue dots represent the measured intersection angle $\varphi_{measure}$ for each fingertip grasp. The critical intersection angles denoted by red dots are applied to distinguishing the stable zone and the unstable zone in Fig. 12(A). The zone below the light-colored surface plotted by the critical intersection angle illustrates the region where the fingertip grasp is quasi-statically stable while the space above the light-colored surface shows the unstable grasp region. With the change from the blue area to the red area of the light-colored surface in Fig. 12(A), the object is increasingly difficult to be grasped steadily by the fingertips. Obviously, objects with the smaller width and the higher thickness are easier to be grasped steadily by the fingertips, as shown in Fig. 12(B).

The intersection angle is measured by us for each test when the gripper performed fingertip grasps so that we can compare these values with ones obtained based on the presented model. In terms of the finger configuration, the first and second joint angle has an effect on the intersection angle together. Thus, the individual angles are not essential. Besides, the under-actuated mechanism used for the gripper lead to the constraints of kinematic transmission and joint rotation for the under-actuated gripper with two 3-link fingers. The gripper can configure its links depending on the existing constraints. Specifically, the relation of the change amounts of three joint angles are given as $\Delta\eta_1 \leq \Delta\eta_2 \leq \Delta\eta_3$ and the rotation ranges of the first, second and third joints are $\frac{\pi}{4} \leq \eta_1 \leq \frac{\pi}{2}$, $\frac{\pi}{4} \leq \eta_2 \leq \frac{\pi}{2}$, and $0 \leq \eta_3 \leq \frac{\pi}{2}$, respectively. Based on the sizes of objects determined by Eq. (30) and Eq. (32), and the gripper constraints mentioned above, the stable and unstable areas for object dimensions are illustrated in Fig. 13. If the width and the thickness of object rest on the unstable areas represented by green areas, an object cannot be grasped steadily (Fig. 13). Otherwise, the fingertips can perform a successful fingertip grasp. Concerning experimental results of grasping three circular objects, the dimensions of the ballpoint pen that cannot be grasped successfully fall in the unstable area. As to objects with other shapes whose dimensions fall in an unstable zone, they cannot be grasped steadily, such as a cell phone, USB drive, and a plate. However, the gripper performs fingertip grasps for other 26 objects successfully, and their dimensions lie in the stable areas.

6. Conclusion

We built a versatile force-form analysis models for evaluating the grasp stability under rolling constraints, providing the theoretical evidence with respect to the fingertip design approach. We evaluated the best fingertip shape and postures relative to the size of the objects that enable a stable grasp by means of constructing mathematical models to describe the effect of fingertip dimension and shape on the stability of fingertip grasp. The geometric relations of the best performing fingertip shape, the sizes of objects and fingertip postures relative to a stable contact point on a plane was indicated as well. The formulation could help researchers in related fields for designing fingertip and/or evaluating fingertip grasping performances, such as a grasp stability, as well as to follow the research line and to further investigate new control strategies. We designed a gripper with two three-phalanges fingers to perform practical experiments for verifying the presented anal-
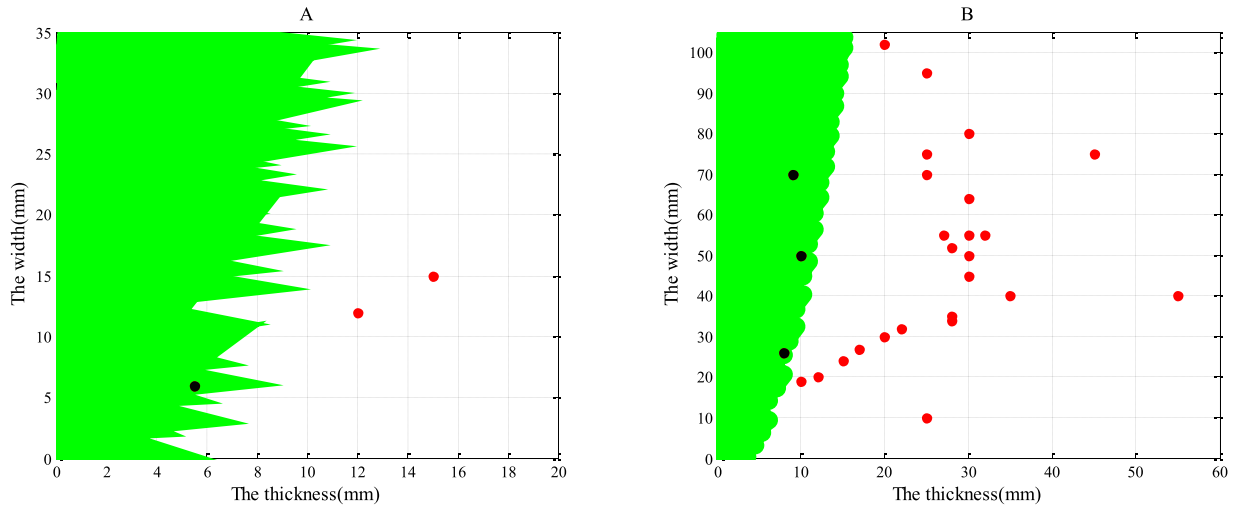
Fig. 13. The unstable grasp area (green) and stable grasp area (white) upon various dimensions of objects with circular shape(A) and other shapes (B). In (A), the diameter is equal to the thickness or the width of object. The coordinates of the solid points represent the dimensions of object. The red points fall in the stable (white) area and the black points rest on the unstable (green) area.The three joint angles are sampled at 0.01 rad for getting dimension ranges.

ysis and model. In the future work, one area we would like to explore is the criteria of the stable precision manipulation performed by an under-actuated robotic gripper with more than two fingers in the 3-dimension domain, and then we will refine the geometric parameters of a robotic gripper to realize more complex manipulations.

Supplementary materials

Supplementary material associated with this article can be found, in the online version, at doi:10.1016/j.mechmachtheory. 2018.08.028.

Appendix

Symbols	nomenclature
TDMs	tendon-driven mechanisms
$\mathbf{J}_k$	the mapping Jacobian matrix from the force dimension to the torque dimension
$\mathbf{F}_t$	the vector of tendon tension force
$\boldsymbol{\tau}$	the joint torque vector
$\mathbf{F}_t$	tendon tension force
F_{ti}	the tension force of each tendon
γ_i	the radius of the ith joint
$\mathbf{J}_i$	the mapping Jacobian matrix from the contact force space to the joint torque space
$\mathbf{F}_i$	the force of the ith contact point regarding the fixed palm frame of reference
k_i	the stiffness
Σ_O	the origin of the object frame of reference
Σ_i^F	the origin of the fingertip frame of reference
δ_i	the compression
(x, y)	the infinitesimal translation
ζ	the infinitesimal rotation
p_i	the displacement
I_2	a 2 × 2 identity matrix
$(\delta_{xi}, \delta_{yi})$	the elastic compression
U	the sum potential energy of two fingers stored in the elastic system
$(\delta_{oxi}, \delta_{oyi})$	the initial compressions at the static equilibrium state
(k_{xi}, k_{yi})	the stiffness constants along the horizontal and vertical directions
(f_{xi}, f_{yi})	the initial grasp forces
∇	Hamiltonian operator
I, J, K	the unit vectors along the orientations of x, y and ζ
H	Hessian matrix
G	the gravity of grasped object
μ	the friction coefficient of contact point
σ	the intersection angle between the direction of contact force and the horizontal direction
λ	the friction angle
σ	the intersection angle between the direction of contact force and the horizontal direction

References

[1] H. Dong, G. Sun, W.-C. Pang, E. Asadi, D.K. Prasad, I.-M. Chen, Fast ellipse detection via gradient information for robotic manipulation of cylindrical objects, IEEE Rob. Autom. Lett. 3 (4) (2018) 2754–2761.
[2] H. Dong, E. Asadi, C. Qiu, J. Dai, I.-M. Chen, Geometric design optimization of an under-actuated tendon-driven robotic gripper, Rob. Comput. Integr. Manuf. 50 (2018) 80–89.
[3] T. Nishimura, K. Mizushima, Y. Suzuki, T. Tsuji, T. Watanabe, Variable-grasping-mode underactuated soft gripper with environmental contact-based operation, IEEE Rob. Autom. Lett. 2 (2) (2017) 1164–1171.
[4] M. Ciocarlie, et al., The Velo gripper: a versatile single-actuator design for enveloping, parallel and fingertip grasps, Int. J. Rob. Res. 33 (5) (2014) 753–767.
[5] A. Bataller, J. Cabrera, M. Clavijo, J. Castillo, Evolutionary synthesis of mechanisms applied to the design of an exoskeleton for finger rehabilitation, Mech. Mach. Theory 105 (2016) 31–43.
[6] N. Robson, G.S. Soh, Geometric design of eight-bar wearable devices based on limb physiological contact task, Mech. Mach. Theory 100 (2016) 358–367.
[7] G.A. Kragten, F.C. Van der Helm, J.L. Herder, A planar geometric design approach for a large grasp range in underactuated hands, Mech. Mach. Theory 46 (8) (2011) 1121–1136.
[8] T. Laliberté, C.M. Gosselin, Simulation and design of underactuated mechanical hands, Mech. Mach. Theory 33 (1-2) (1998) 39–57.
[9] L. Birglen, T. Laliberté, C.M. Gosselin, Underactuated Robotic Hands, Springer, 2007.
[10] D.J. Montana, Contact stability for two-fingered grasps, IEEE Trans. Rob. Autom. 8 (4) (1992) 421–430.
[11] E. Rimon, J.W. Burdick, Mobility of bodies in contact. II. How forces are generated by curvature effects, IEEE Trans. Rob. Autom. 14 (5) (1998) 709–717.
[12] Y. Funahashi, T. Yamada, M. Tate, Y. Suzuki, Grasp stability analysis considering the curvatures at contact points, in: Robotics and Automation, 1996. Proceedings., 1996 IEEE International Conference on, vol. 4, IEEE, 1996, pp. 3040–3046.
[13] T. Yamada, R. Johansson, A. Robertsson, H. Yamamoto, Static stability analysis of a planar object grasped by multifingers with three joints, Robotics 4 (4) (2015) 464–491.
[14] T. Yamada, T. Taki, M. Yamada, Y. Funahashi, H. Yamamoto, Static stability analysis of spatial grasps including contact surface geometry, Adv. Rob. 25 (3–4) (2011) 447–472.
[15] T. Yamada, H. Yamamoto, Grasp parameter effect for static grasp stability of a single planar object, in: SICE Annual Conference (SICE), 2013 Proceedings of, IEEE, 2013, pp. 294–300.
[16] E. Rimon, J.W. Burdick, New bounds on the number of frictionless fingers requied to immobilize, J. Field Rob. 12 (6) (1995) 433–451.
[17] E. Rimon, J.W. Burdick, T. Omata, A polyhedral bound on the indeterminate contact forces in planar quasi-rigid fixturing and grasping arrangements, IEEE Trans. Rob. 22 (2) (2006) 240–255.
[18] E. Rimon, R. Mason, J.W. Burdick, Y. Or, A general stance stability test based on stratified morse theory with application to quasi-static locomotion planning, IEEE Trans. Rob. 24 (3) (2008) 626–641.
[19] D.J. Montana, The kinematics of contact and grasp, Int. J. Rob. Res. 7 (3) (1988) 17–32.
[20] M. Yoshida, S. Arimoto, K. Tahara, Pinching 2D object with arbitrary shape by two robot fingers under rolling constraints, in: Intelligent Robots and Systems, 2009. IROS 2009. IEEE/RSJ International Conference on, IEEE, 2009, pp. 1805–1810.
[21] J. Wu, R. Dong, Analysis of the contact interactions between fingertips and objects with different surface curvatures, Proc. Inst. Mech. Eng. Part H J. Eng. Med. 219 (2) (2005) 89–103.
[22] H. Maekawa, K. Tanie, K. Komoriya, Kinematics, statics and stiffness effect of a 3D grasp by multifingered hand with rolling contact at the fingertip, J. Rob. Soc. Jpn 16 (2) (1998) 205–213.
[23] K. Hang, et al., Hierarchical fingertip space: a unified framework for grasp planning and in-hand grasp adaptation, IEEE Trans. Rob. 32 (4) (2016) 960–972.
[24] S. Krut, V. Bégoc, E. Dombre, F. Pierrot, Extension of the form-closure property to underactuated hands, IEEE Trans. Rob. 26 (5) (2010) 853–866.
[25] G.A. Kragten, J.L. Herder, The ability of underactuated hands to grasp and hold objects, Mech. Mach. Theory 45 (3) (2010) 408–425.
[26] A. Bicchi, On the closure properties of robotic grasping, Int. J. Rob. Res. 14 (4) (1995) 319–334.
[27] G.A. Kragten, J.L. Herder, Equilibrium, stability, and robustness in underactuated grasping, in: Proc. of the ASME, 2007.
[28] M. Bélanger-Barrette, ROBOTIQ Collaborative Robot eBook, 15, 2015.
[29] R. Ozawa, H. Kobayashi, K. Hashirii, Analysis, classification, and design of tendon-driven mechanisms, IEEE Trans. Rob. 30 (2) (2014) 396–410.
[30] M. Russo, et al., Design and test of a gripper prototype for horticulture products, Rob. Comput. Integr. Manuf. 44 (2017) 266–275.
[31] L.L. Howell, S.P. Magleby, B.M. Olsen, Handbook of Compliant Mechanisms, John Wiley & Sons, 2013.
[32] V.-D. Nguyen, Constructing stable grasps, Int. J. Rob. Res. 8 (1) (1989) 26–37.
[33] E. Rimon, J.W. Burdick, New bounds on the number of frictionless fingers required to immobilize 2D objects, in: Robotics and Automation, 1995. Proceedings., 1995 IEEE International Conference on, vol. 1, IEEE, 1995, pp. 751–757.
[34] Y.-B. Jia, Grasping curved objects through rolling, in: Robotics and Automation, 2000. Proceedings. ICRA'00. IEEE International Conference on, vol. 1, IEEE, 2000, pp. 377–382.
[35] R. García-Rodríguez, M. Villalva-Lucio, V. Parra-Vega, Dexterous dynamic optimal grasping of a circular object with pose regulation using redundant robotic soft-fingertips, in: Intelligent Robots and Systems (IROS), 2015 IEEE/RSJ International Conference on, IEEE, 2015, pp. 6231–6237.
[36] V.-D. Nguyen, Constructing force-closure grasps, Int. J. Rob. Res. 7 (3) (1988) 3–16.